Master degree on Nanostructured Materials for Nanotechnology Applications

USE OF HIGHLY CONJUGATED ORGANIC COMPOUNDS FOR THE FABRICATION OF METAL / MONOLAYER / METAL DEVICES

Jorge Trasobares Sánchez

SEPTEMBER 2012

PILAR CEA MINGUEZA profesor titular del Departamento de Química Física de la Universidad de Zaragoza y SANTIAGO MARTÍN SOLÁNS, contratado Ramón y Cajal del Departamento de Física de la Materia Condensada de dicha Universidad

CERTIFICAN:

Que el trabajo presentado en esta memoria por Jorge Trasobares Sánchez como Proyecto Final del Máster Universitario en Materiales Nanoestructurados para Aplicaciones Nanotecnológicas y que lleva como título "Use of highly conjugated organic compounds for the fabrication of metal / monolayer / metal devices", ha sido realizado en el Departamento de Química Física de la Facultad de Ciencias de la Universidad de Zaragoza, bajo su dirección, autorizando la presentación de la misma para su calificación por el Tribunal correspondiente.

Y para que así conste, se expide el presente certificado, en Zaragoza, a 3 de septiembre de 2012.

Fdo: Pilar Cea Mingueza Fdo: Santiago Martín Soláns

Content

Resume

The progressive miniaturization of the components used in electronic devices has allowed the development of technology as it has been described by Moore's law. However, silicon technologies is reaching the limits of miniaturization; thus, exploring new fields is necessary to progress in the manufacture of smaller, more efficient and with new properties devices. Molecular electronics is presented as an important technology for developing a hybrid technology (Si-electronics) in the near future and projecting a complete replacement of silicon technology in a far future.

On the other hand, with the emergence of sophisticated assembly techniques as a consequence of the progress in Nanoscience, it is expected that molecular electronics maintain the current miniaturization process. Therefore, this project is focused on the assembly of molecules by the Langmuir-Blodgett technique with special attention on one of the challenges set by the ITRS (International Technology Roadmap for Semiconductors): the fabrication of a top electrode contact onto an organic monolayer without damaging it.

To achieve this objective, this work presents three different approaches. The first one, is the rupture of an organometallic compound containing a gold atom in the backbone; the breakdown of these molecules by annealing produce the reduction of the gold atom generating gold nanoparticles which remain onto the monolayer acting as the top metal electrode. The second approach is to use the new technology "Stencil Lithography". This lithography consists on using a mask for evaporating small amounts of metal onto a monolayer, minimizing the possibility of generating a short circuit. Finally, we have studied the formation of graphene oxide monolayers by Langmuir-Blodgett technique; these monolayers would be deposited on an organic monolayer and after reduction acts as the top semiconductor electrode.

1 Introduction

This work, which constitutes the final master project of the Master in Nanostructured Materials for Nanotechnology Applications of the Zaragoza University, has been developed at the Physical Chemistry Department of Zaragoza University and also at the National Center of Microelectronics of Barcelona (CNM-CSIC). The objective of this project is to open new research lines to provide some insight into one of the most challenge bottlenecks in molecular electronics: the construction of the top-contact electrode without inducing any damage to the organic monolayer beneath. To do so, both top-down and bottom-up approaches have been used.

In the next section a review of the State of the Art on molecular electronics is presented together with the objectives of this work. In chapter 2, the experimental procedures, together with the main techniques and materials used along this project are shown, in chapter 3, the experimental results for the rupture of a metal organic compound to form the top-contact electrode are presented, and in chapter 4, the results related to the deposition of a metal layer by stencil lithography are reported. In chapter 5, graphene is presented as a possible alternative to form the top-contact electrode. Finally in chapter 6 summarizes the conclusions of this work.

1.1 Revision of the State of the Art

Manipulating matter on an atomic scale, arbitrarily located between 100 and 0.1 nm[1], is a key technology for the present and the future which is known as Nanotechnology. Accordingly, billions of dollars have been invested in research areas related to Nanotechnology with an exponential grown in the number of publications [2-3]. Nevertheless, Nanotechnology is not exactly new; as one goes deeper into the subject more old uses of the properties of matter at nanoscale one can find. For example, nanoparticles (NPs) of gold and silver coloring of clear-cut yellow, red or blue stained glass windows of medieval churches, where color depends on the nature and diameter of the NPs. Romans also hid their white hair applying a paste of chalk and lead oxide

(procedure not recommended due the lead toxicity, but interesting because the reaction of the sulfur in hair reacts with the oxide, growing black nanocrystals of lead sulfide).

It was Richard Feynman the first scientist to notice that there is nothing in physics that prevents the use of atoms and molecules as if they were bricks with which to construct molecular buildings. His famous lecture at the American Physical Society Meeting at Calttech on the 29th December 1959 is well known. Scientific research groups are attracted by the possibility of direct manipulation of individual atoms or molecules and companies are interested in the profits that this knowledge can offer. Although Richard Feynman suggested the possibility of making nanoscale machines, the term Nanotecnology (first used by Norio Taniguchi, 1974) was popularized by K. Eric Drexter in his popular 1986 book, "Engines of Creation: The Coming Era of Nanotechnology". This author suggested that these tiny machines could make copies of themselves via computer control instead of being control by human operators [2].

There are many different and multidisciplinary fields of applications of Nanotechnology and the ability to build with atomic precision has already let developing materials with new and improved magnetic, tensile, thermal and electrical properties. A lot of sectors are benefited of this knowledge, such as medicine (e.g. drug delivery systems or medical diagnostic tools, such as cancer tagging mechanisms and lab on a chip providing real time diagnostics); energy and environment where nanostructured photovoltaic cells are being developed as well as filters incorporating NPs which have excellent properties for liquid filtration. Textile industry, production of artificial skin and muscles among others fields also take advantage of the Nanotechnology [4]. Another important field of applications is Nanoelectronics, which studies the phenomena of transport and distribution of charge and spin on the nanometer scale [5]. This project is intimately related to the field of Nanoelectronics, and more specifically, on Molecular Electronics which hunts for incorporating molecular components as functional elements in electronic devices [6].

Moore´s Law was coined around 1970 by the Caltech professor Gordon Earl Moore. In his publication "Cramming more components onto integrated circuits" [7] Electronics Magazine 19th April 1965 we can read that "The complexity for minimum component costs has increased at a rate of roughly a factor of two per year..." it means

that the number of transistor can be doubled every year. In 1975, Moore altered his projection to a doubling every two years.

Consequently with this miniaturization, the International Technology Roadmaps for Semiconductor (ITRS) [8], which gives guidance on research and development in the semiconductor field, notices three main research domains in its Nanoelectronics Roadmap, called: "More Moore", "More than Moore" and "Beyond CMOS[1]", Figure 1.1. These two latter domains evade the aggressive Moore's law which is not anymore the unique or the main driver.

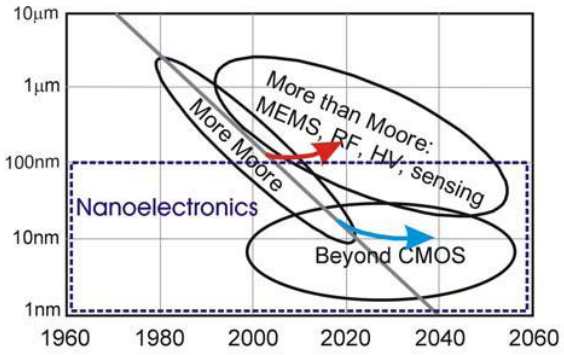

Figure 1.1. Scheme suggesting in a qualitative way the evolution of the device size relevant to this division of nanolectronics [9].

The first domain, called "More Moore", trends for increased performances with technologies related to the nanometer CMOS. This trail has been leading the silicon technology, but its time is close to be over due to technological reasons. In addition, the huge investments needed to build new production lines in this silicon technology are expected to be so high that this technology might not be profitable in the near future. At least in the next 15 or 20 years, the use of dielectrics like Hafnium or the optimization of the surface into a wafer is not enough to front some significant limitations to this technology [10].

The second trend is designated as "Moore than Moore". It is characterized by functional diversification of semiconductor-based devices. These non-digital functionalities do contribute to the miniaturization of electronic systems, although they do not necessarily scale at the same rate as the one that describes the development of digital functionality. This domain based on the engineering of complex systems

[1] CMOS: Complementary Metal-Oxide-Silicon

combines various technologies (not exclusively electronics) in order to meet certain needs and challenging specifications of advanced applications.

Finally, the "Beyond CMOS" domain, addresses with disruptive technology and device principles with the ability to scale the functional performances of information processing beyond the ones of ultimately scaled CMOS in order to truly exploit atomic-scale technology (from semiconductor to molecular technology). Novel switches, architectures for universal memory and new interconnect approaches are some of the identified targets.

In this context, Molecular Electronics pursues the use of molecules to build up electronic devices which in the future might substitute the conventional CMOS devices. Molecular Electronics involves the study and application of molecular building blocks for the fabrication of electronic components using monomolecular films incorporating functional organic materials as well as single-molecule electronic components. The assembly of molecular building blocks for the fabrication of electronic components includes both passive (e.g. resistive wires) and active components such as transistors and molecular-scale switches.

The seminal work from Aviram and Ratner in 1974 is considered the origin of molecular electronics. This contribution generated many expectations about preferential conduction in one direction in molecular materials. Additionally, conductive polymers and some basic ideas about the electronic behavior of organic compounds were emerging in the literature of the time. A remarkable event was the discovery of conductive polymers, awarded with the Nobel Prize in Chemistry in 2000 shared by Alan J. Heeger [11], Alan G. Mac Diarmid [12] and Hideki Shirakawa[13].

Some organic materials have been demonstrated to offer electrical properties similar to those of metals and semiconductors, but with improved mechanical properties, processing advantages and low production costs. Organic molecules assembled into electronic devices can offer advantages such as their small size, high speed of process, low costs of fabrication, less consume, etc. Limitations include the low stability of organic materials at high temperatures [14-15] and the necessity of fabricating exceptional robust contacts between metal and molecules.

In 2009 the International Technology Roadmap for Semiconductor, ITRS [8], has pointed out the main bottlenecks that should be overcome before Molecular Electronics can be incorporated in the market. The most important challenges in molecular electronics are:

- Look for new metal/molecules interfaces in order to get efficient contacts.
- Understand and control the behavior of metal/molecules/metal interfaces under an electric field.
- Developing easy, robust, and efficient methods to deposit the top-contact electrode onto the organic monolayer without damage of the monolayer and without penetration of the metal through the organic material producing a short circuit.
- Define protocols or design assembly strategies for precise placement of molecular materials within device structures.

The research group Platon at the University of Zaragoza is working on these challenges. In particular this project is focused on the development of new alternatives for the fabrication of the top-contact electrode. Therefore, in the following lines, a revision of the main methods used in the literature for the deposition of this top-contact electrode is presented together with their limitations which highlight the need of finding new protocols for the deposition of the second electrode.

Until now there is no technique to achieve a robust contact between the molecule and the top-contact electrode [16]. It is possible to evaporate directly the metal over the monolayer however generally short-circuits are formed in this process due to the penetration of the metal through the monolayer and contact with the underlying electrode. In order to decrease the energy of the metal atoms when reach the monolayer surface there are some alternative methods such as: refrigeration of the substrate (~100 K), introduction of an inert gas in the evaporator chamber or the use of deflectors that block the direct pass from the evaporator to the sample [17-18].

Another approach consists on the deposition of a drop of mercury on the monolayer; the equipment is simple and due to the high surface tension of mercury no penetration of the metal through the layer occurs. However, mercury tends to form oxides which change the electrical properties of the devices and additionally mercury

ions can be formed and then penetrate the layer. Moreover the contact area between the mercury and the layer changes depending on applied voltage [19-20]. In addition, due to the liquid nature of mercury, this technique is nor particularly interesting for permanent contacts in real devices.

Conductive polymers can be deposited onto the organic layer in order to avoid penetration of the metal, but the polymer can penetrate through the layer and generate a short-circuit as well [21]. Similarly carbon nanotubes can be deposited onto the layer but the procedure has experimental difficulties [22]. Finally better results have been achieving using graphene to protect the layer [23].

In order to prevent the damage suffered by the layer when the top electrode is transferred, a sacrificial substrate can be used. A normal sacrificial substrate is PDMS (polydimethylsiloxane) which can be patterned with nanomotives by lithographic techniques. Gold can be evaporated onto PDMS and then a thiol layer is put in contact with the gold layer. As the force between thiol and gold is stronger than the force between the PDMS and gold then it is possible to retire the PDMS obtaining a metal/molecule/metal device. The mayor limitation is that the terminal group of the molecules must form stronger links with the metal than the PDMS forms with this metal. Besides, the force applied has to be controlled not to damage the molecular layer. There are other methods such as "lift-off, float-on" [24] and the "polymer-Assisted Lift-Off"[25-26] which also use a sacrificial substrate but use water to separate the metal.

Finally "Surface-Diffusion-Mediated Deposition" method implanted by Bofinas and col. [27] has been reaching good results, evaporating gold over a SiO_2 protector layer which prevents the damage and then facilitating the superficial diffusion of the atom until the top of the molecular layer.

Nevertheless, experimental methods need to be improved to make this top-contact. This remains a very active area of research both in terms of basic and applied science.

1.2 Objectives

The main objective of this project is to find new protocols for the deposition of the top contact electrode onto mono-molecular films without damaging the molecule or penetration of the second metal through the organic film. In particular, three different procedures are explored and discussed:

1. Rupture of a metal-organic compound (MOC). A monomolecular layer of a MOC specially designed for this work is assembled using the Langmuir-Blodgett (LB) technique; then the film is annealed with the purpose of breaking the molecule and form gold nanoparticles onto the molecular layer which behave as the top contact electrode. To our knowledge, this method has not been reported before in the literature and offers promising applications.

2. Use of stencil lithography. A thin gold layer is evaporated using stencil lithography onto monomolecular LB films to form metal/molecule/metal devices. Electrical measurements have been done to determine the rate of short-circuits and to compare the results with traditional evaporation methods.

3. Fabrication of graphene oxide layers by the LB method. Graphene oxide compatibility with Langmuir-Blodgett technique is studied. Formation of graphene oxide layers (1-4 monolayers) at the air-water interphase is demonstrated, and consequently could be used for the fabrication of the top-contact electrode by transference onto monomolecular films and subsequent reduction.

2 Experimental procedures

In this chapter the materials used for the realization of this project are presented; firstly, the functional materials that have been assembled into thin solid films to build the electronic devices; secondly, solvents, solutions and substrates used to carry out this work and finally another important material used in the development of this project, graphene oxide. In this section we will also revise the main techniques used: Langmuir-Blodgett (LB) and Stencil Lithography (SL) methods; as well as the characterization techniques: Brewster Angle Microscopy (BAM), UV-vis reflection spectroscopy, Atomic force microscopy (AFM), Quartz Cristal Microbalance (QCM), Optical Microscopy, X-Ray Photon Spectroscopy (XPS), and Scanning Electron Microscopy (SEM) are briefly presented.

2.1 Materials

Figure 2.1 shows the structure of the organic molecule used in this work, 4-methoxy-isocyanidebencene)-[[4-{(4-aminophenil)ethynyl}phenyl]ethynyl]-gold, abbreviated as MeOPhAu-Tolan-NH_2. This material was synthesized at the Chemistry Department of Durham University (UK) by Professor Paw J. Low.

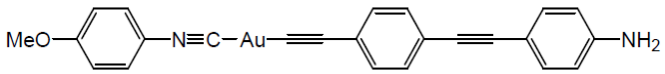

Figure 2.1. Chemical structure of the organic compound used in this work. (4-methoxy-isocyanidebencene)-[[4-{(4-aminophenil)ethynyl}phenyl]ethynyl]-gold, abbreviated as MeOPhAu-Tolan-NH_2.

Table 2.1 shows the solvents used in this work as well as their CAS number, purity and supplier. Milli-Pore Milli-Q water was used as subphase in the LB technique; chloroform was used to solve the organic compounds; ethanol and methanol were the solvents for graphene oxide solutions; acetone was used as a cleaning solvent and nitrogen was used to dry the substrates. In table 2.2, the substrates used to carry out the

transference of the Langmuir films as well as the supplier, the cleaning protocol and their uses are indicated.

Table 2.1. Solvents used in this work.

Compound	CAS number	Purity	Purchased from
Water		Milli-Pore Milli – Q (resistivity 18.2 MΩ·cm)	Obtained from the Faculty of Science Distillator
Chloroform	67-66-3	99 % (ethanol 1 %)	Sigma-Aldrich
Ethanol	64-17-5	99.5 %	Panreac
Methanol	67-56-1	99.8%	Panreac
Acetone	67-64-1	99.5 %	Panreac
Nitrogen	7727-37-9	99.999 %	Linde

Table 2.2. Substrates on which the LB films were deposited.

Name	Purchased from	Cleaning protocol	Used for
Mica	Ted Pella, Inc.	Exfoliated and rinsed with ethanol	Topography characterization by AFM
Quartz substrates covered with gold	Stanford Research Systems	Cleaned with water MilliPore Milli – Q and dried with N_2	Quartz Crystal Microbalance
Gold	Arrandee®	Annealed to produce Au (111), rinsed with ethanol and dried with N_2	Conductance measurements in Metal/ molecule/ Metal devices
Quartz	Hella Analytics	15 minutes in chloroform and ultrasounds. Dried with N_2. 4 times 15 minutes cleaned with water MilliPore Milli – Q and ultrasounds, rinsed dried with N_2	X-Ray Photoelectron Spectroscopy (XPS)

Finally, other objective of this project is to verify the possibility of assembling Graphene Oxide (GO) by means of the LB method. These GO layers would be subsequently reduced to produce reduced graphene oxide, which has similar properties to graphene. Graphene is a promising material with a large number of applications including its uses as a transparent top electrode [28]. Graphene oxide dispersions 23 $mg \cdot mL^{-1}$ in a 5:1 methanol:water and 5:1 ethanol:water mixture solutions were kindly provided by Professor María Teresa Martinez, Dr. Ana Benito and Dr. Wolfrang Maser from the "Instituto de Carboquímica" CSIC.

2.2 Fabrication and Characterization Techniques

2.2.1. Fabrication techniques

Langmuir-Blodgett (LB)

LB technique is a sophisticated method that permits the fabrication of high-ordered films composed by one or several layer. A Langmuir film is prepared by spreading a dilute solution of an amphiphilic material onto a liquid surface. Under these conditions, molecules are able to form a stable monolayer at the air-water interface by anchoring the polar group at the water surface whilst the hydrophobic part of the molecule provides stability to the system thanks to lateral molecular interactions (van der Waals or π-π interactions). Once a stable monolayer has been formed at the air-water interface, this film can be transferred onto a solid substrate giving mono or multilayered films which are named Langmuir-Blodgett (LB) films.

This project has been carried out in the laboratory of the Platon´s Group belonging to Physical Chemistry Department of Zaragoza University. This lab is equipped with five Langmuir troughs, see a general scheme of a trough in Figure 2.2. Two of them are homemade and the others ones commercial; by NIMA and KSV. All these troughs are housed in a constant temperature (20 ± 1 ºC) cleaned room. A Wilhelmy paper plate pressure sensor was used to measure the surface pressure (π) of the monolayers [29]. The sub-phase was Milli-Pore Milli-Q water (resistivity 18.2 MΩ·cm). To construct the Langmuir films a diluted solution of the organic material in chloroform was spread using a Hamilton syringe held very close to the surface, allowing the surface pressure to return to a value close to zero between each addition. After waiting about fifteen minutes to allow the solvent to evaporate completely, slow compression of the film began at a speed of 0.022 $nm^2 \cdot molecule^{-1} \cdot min^{-1}$. The surface pressure-area isotherm was recorded upon the compression process. Other *in situ* characterization techniques, described below, were used including surface-potential isotherms, Brewster Angle Microscopy and UV-vis spectroscopy.

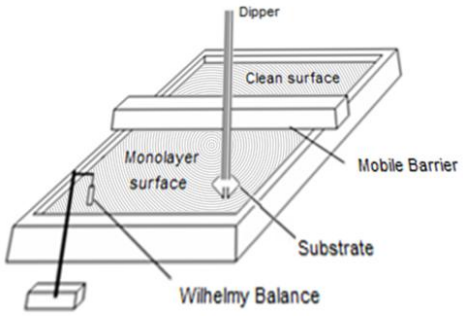

Figure 2.2. Simplified scheme of a Langmuir-Blodgett though.

Stencil Lithography (SL)

Stencil Lithography (SL) is a direct vacuum patterning technology where a controlled amount of the desired material is directly deposited only where it is required through the stencil[2] apertures without the need of additional processing steps such as, for example, those used in photolithography. SL requires only a few process steps compared to photolithography and lift-off process in which most of organic semiconductors and flexible polymeric substrates cannot withstand due to the heat load and chemical interactions involved in these steps.

2.2.2. Characterization techniques

Brewster Angle Microscopy (BAM)

A direct visualization of Langmuir films is possible by means of the Brewster Angle Microscope (BAM). In this work the equipment used is a micro-BAM from KSV-NIMA (50 mW, 659 nm), having a lateral resolution better than 12 μm. In the BAM a laser beam (*p*-polarized) is focused onto the surface [30]. If the incident angle is equal to the so called Brewster angle, α, then no light is reflected, and black pictures are recorded by the analyzer. The Brewster Angle is defined according to the Snell law as [31].

[2] Stencil: It is a thin sheet of material in which has been designed a patter. Stencil is used to reproduce these patters on an underlying surface by applying a pigment through the cut-out holes in the material. The main advantage of this technique is that stencil can be reusable.

$$tg\ \alpha = \frac{n_2}{n_1} \qquad (1)$$

where α is the Brewster angle and n_1 and n_2 are the refraction index of air and water, respectively.

When the monolayer is spread onto the water surface and the angle of incidence is kept constant, a small part of the incident light beam is reflected due to the floating material (change in the refraction index) and by means of appropriated software, pictures of the monolayer can be obtained. The photographs show different levels of grey depending on the monolayer thickness and orientation.

UV-Vis reflection spectroscopy

Reflection spectroscopy allows determining the presence and orientation of chromophore units on the surface. The measurements were performed using the spectrophotometer RefSpec Nanofilm (Göttingen, Germany). The light source is a lamp DTM FiberLight 6/50 comprises two deuterium and tungsten lamps installed in a ceramic sensor. The working range of the spectrophotometer is 240 to 1000 nm.

The reflection spectroscopy technique consists on radiation impinging perpendicularly on the surface (a light trap is placed inside the aqueous subphase to avoid contamination by reflection from said subphase). The reflection does not change significantly unless the molecules absorb radiation, but when the molecules absorb the reflection increases according with equation 3:

$$(R_{D,S} - R_D) = \Delta R = A_D\sqrt{R_S} \qquad (2)$$

where R_S and $R_{D,S}$ represent the intensity of the beam reflected by the aqueous surface before and after the film formation, respectively; ΔR is the variation of the radiation and A_D is the absorbance characteristic of the monolayer. This equation is only valid for small values of A_D. The parameters to determine experimentally are $R_{D,S}$ and R_S, meanwhile ΔR is obtained directly. Equation 3 shows a linear dependence of the increase of the reflection respect to the chromophore density at the interface. A reflection spectrum has the same shape as an absorption spectrum.

Quartz Crystal Microbalance (QCM)

Quartz Crystal Microbalance measurements were carried out using a Stanford Research Systems instrument. The sensor is a thin disk of α-quartz, with a thickness of about 331 μm, which is cut in the direction AT (35° 15'). The circular disc presents gold electrodes on both sides and its nominal frequency of oscillation is ca. 5 MHz. Due to the piezo-effect, an AC voltage across the electrodes induces a shear deformation and vice versa. By using the Sauerbrey equation [32] the variation in mass can be determined (and consequently the surface density of the film deposited onto the QCM substrate):

$$\Delta f = -\frac{2 f_0^2 \Delta m}{A \rho_q^{1/2} \mu_q^{1/2}} = -Cf \cdot \Delta m \qquad (3)$$

where f_0 is the fundamental resonant frequency of 5 MHz, Δm is the mass change (g), A is the electrode area, ρ_q is the density of the quartz (2.65 g·cm^{-3}), and μ_q is the shear modulus ($2.95 \cdot 10^{11}$ dyn·cm^{-2}).

Atomic Force Microscopy (AFM)

Atomic Force Microscopy is one of a large number of scanning probe microscope methods (SPMs) which permits the determination of images of a surface using a physical probe which scans the sample. The scanning is obtained by mechanically moving the probe, line by line, and recording the probe-surface interaction as a function of the position. There are two modes of operation: contact mode and tapping mode. In this work, the images of the monomolecular films were obtained using an AFM Multimode 8 (Veeco) belonging to the Laboratory of Advanced Microscopies (LMA). The characterization of the films was carried out using the tapping mode with a silicon tip from Bruker with a resonance frequency of 300 kHz and a constant force of 40 mN and a sweep rate of 1 Hz. To perform the electrical measurements a Veeco conducting AFM (C-AFM) belonging to the CNM was used in contact mode, applying a voltage from -4 to 4 V.

Optical microscopy

Optical microscopy is a type of microscopy which uses light and a system of lenses to magnify images of small samples. In this work, a Nikon Eclipse ME600 is used to check the state of stencil shadows and also to localize the top-electrodes deposited through them.

Scanning Electron Microscopy (SEM)

Scanning Electron Microscopy (SEM) is a type of electron microscope which images a sample by scanning it with an electron beam. Electrons interact with atoms in the sample resulting in the emission of secondary or back-scattered electrons, which provide information about the topography and composition of the sample.

The equipment used in this work is a JEOL JSM 6400 instrument which belongs to the Laboratory of Advanced Microscopies (LMA). The resolution is 3.5 nm using a 35 keV electron beam and a focal distance of 8 mm.

X-Ray Photoelectron Spectroscopy (XPS)

The measurements were carried out using a Kratos AXIS Ultra DLD spectrometer with a monochromatic X-ray source of aluminum [Al Ka (1486.6 eV)]. The spectrometer is located in the laboratories of the Institute of Nanoscience of Aragon (INA). The XPS spectra are obtained when a sample is irradiated with X-rays while the kinetic energy is measured and the number of electrons is stripped from the analyzed surface. Finally, the analysis photoelectrons energies and intensities provide information of the oxidation state of certain constituents of the material incorporated in the film.

3 Rupture of a Metal organic compound to form the Top contact electrode

In this section, the results obtained for one of the strategies used to form the top contact electrode, rupture of a metal organic compound, are showed. The molecule chosen for carrying out this study was presented in chapter 2 as well as the technique used to ensemble this compound: the Langmuir-Blodgett method.

Additionally to the condition exposed in chapter 2, in this section a MeOPhAu-Tolan-NH_2 10^{-5} M in chloroform was used and a volume of the spreading solution that yields an initial surface coverage of 1.25 $nm^2 \cdot molecule^{-1}$. In addition, the solution was sonicated for 10 minutes before the spreading process to minimize aggregation phenomena. Figure 3.1 shows a reproducible surface pressure-area per molecule (π-*A*) isotherm of MeOPhAu-Tolan-NH_2 at the air-water interface. The π-*A* isotherm is characterized by a zero surface pressure in the 1.4-0.45 $nm^2 \cdot molecule^{-1}$ range, featuring a lift-off at 0.45 $nm^2 \cdot molecule^{-1}$ followed by an increase of the surface pressure upon compression. Changes in the slope reveal a progressive orientation and/or reorientation of the molecules at the interface during compression.

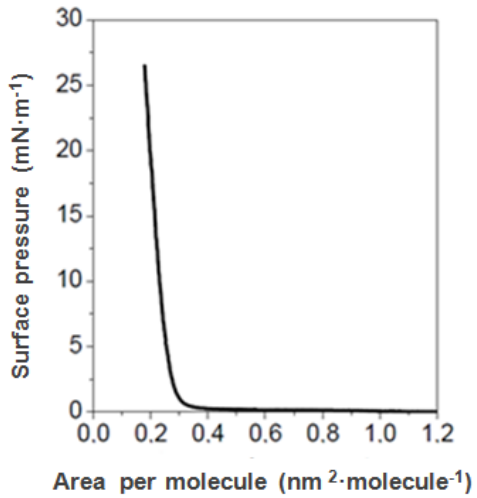

Figure 3.1. Surface pressure vs. area per molecule (π-A) isotherm of MeOPhAu-Tolan-NH_2 at 20 ºC.

Brewster angle microscopy (BAM) images were recorded upon compression process of the monolayer to get more information about its characteristics, Figure 3.2. It is important to note here that in spite of the tendency of this compound to aggregate as a consequence of π-π lateral interactions and aurophilic lateral interactions between MeOPhAu-Tolan-NH_2 molecules no three-dimensional aggregates were observed in BAM images under the experimental conditions used to fabricate these films. Nevertheless, a rapid increment in the brightness of the images upon compression after the lift-off is observed indicating that the film thickness of the monolayer increases. In addition, at higher surface pressures (e.g., 14 $mN \cdot m^{-1}$) BAM images show that the monolayer covers practically all the water surface.

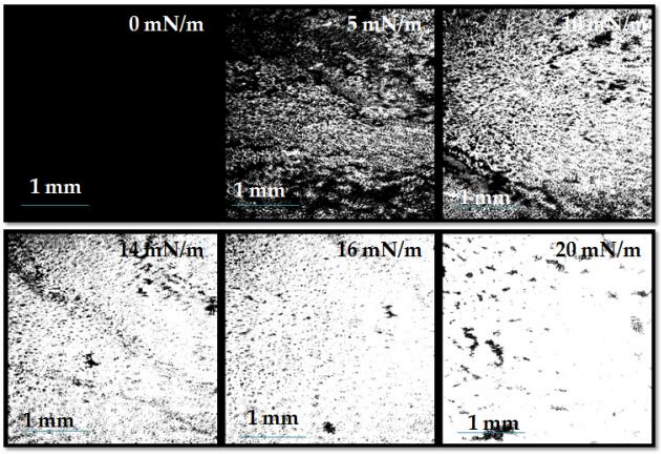

Figure 3.2. BAM images of MeOPhAu-Tolan-NH_2 at the air-water interface at the indicated surface pressures.

Molecular organization of Langmuir films upon compression was investigated in situ by UV-vis reflection spectroscopy through the reflection of light under normal incidence. A normalized spectrum is used to eliminate the dependence with the surface density (ΔR_{norm}= $\Delta R \cdot$Area per molecule in which the ΔR is the reflection). Normalized spectra are showed in Figure 3.3.

As can be observed, the intensity of the normalized spectra decreases upon compression of the monolayer until a surface pressure of 16 $mN \cdot m^{-1}$ revealing a more vertical orientation of the molecules respect to the air-water interface during the compression process. At higher surface pressures, the general trend is not fulfilled and the normalized reflection spectra intensity increases slightly or keeps constant indicating that the collapse of the monolayer could have been achieved.

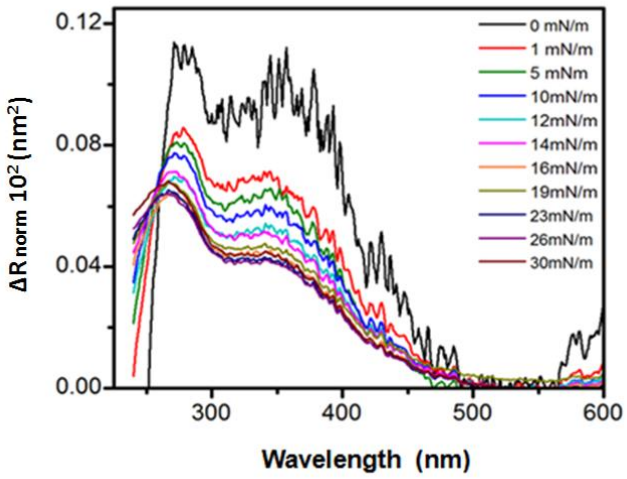

Figure 3.3. Normalized reflection spectra of MeOPhAu-Tolan-NH_2 upon compression at the indicated surface pressures.

According to the results obtained, we can say that an adequate surface pressure to transfer the Langmuir layer onto a substrate could be 14 $mN \cdot m^{-1}$. In addition, monomolecular films were transferred onto mica at several surface pressures to corroborate the optimum surface pressure of transference and to check the morphology of the LB films.

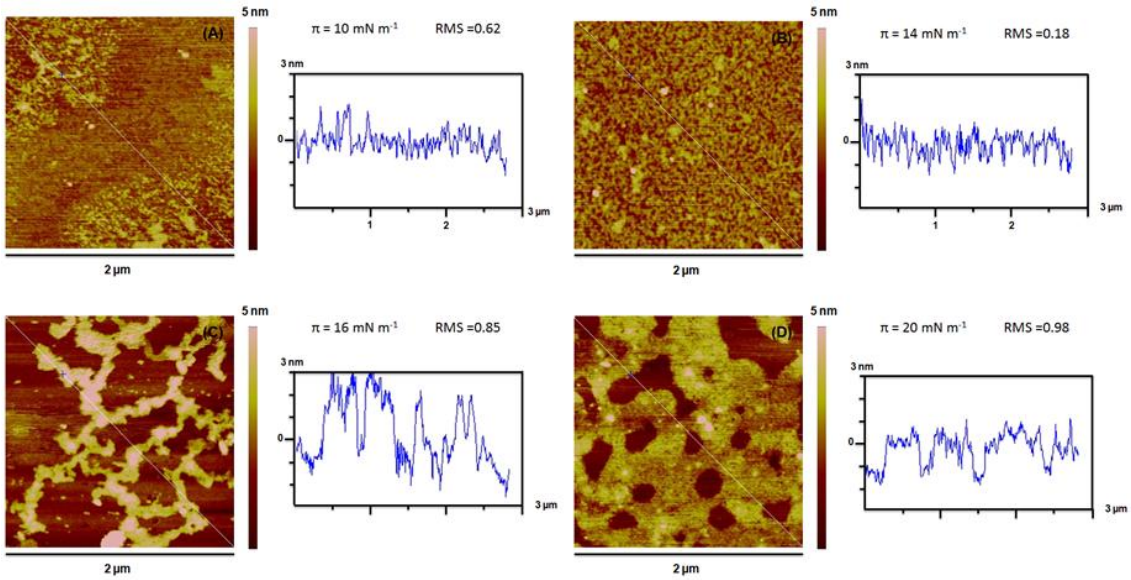

Figure 3.4 *AFM images and sections of a one-layer LB film of MeOPhAu-Tolan-NH_2 transferred at the indicated surface pressures. Root mean square (RMS) roughness values are also indicated for each film.*

The optimum surface pressure to transfer the Langmuir layer onto a substrate was demonstrated to be 14 $mN \cdot m^{-1}$ since lower or higher surface pressures yield to films with a higher root mean square (RMS) roughness and the evidence of holes or three dimensional aggregates in the film, see Figure 3.4. In addition, atomic force microscopy images also revealed the formation of highly homogeneous films with low defect densities at 14 $mN \cdot m^{-1}$.

Therefore, Langmuir monolayer were transferred onto solid substrates, initially immersed in the sub-phase, by vertical dipping method at the surface pressure of 14 $mN \cdot m^{-1}$. One or several layers can be transferred by this method, see table 3.1. At this surface pressure, the transfer ratio (the relationship between the surface coverage of the monolayer at the air-water interface and the surface coverage in the substrate) was 1. The experimental surface coverage as well as the transfer ratio was also verified by the QCM; the frequency change (Δf) for a QCM substrate before and after the transference (Δf = - 48 Hz) provides the mass change (Δm) making use of the Sauerbrey equation, equation 2.2. With this value a surface coverage of $\Gamma = 4.68 \cdot 10^{14}$ $molecules \cdot cm^{-2}$ was obtained. The theoretical surface coverage is given from the molecular area of the MeOPhAu-Tolan-NH_2 monolayer at the air-water interface at the surface pressure of 14 $mN \cdot m^{-1}$ which is $\Gamma = 4.76 \cdot 10^{14}$ $molecules \cdot cm^{-2}$. This result confirms that the transfer ratio is close to 1.

Table 3.1. Transference ratios calculated by QCM for several layers.

Nº layer	T**ransferenc**e ratio
1	**1,018**
2	**0,997**
3	**0,997**
4	**0,958**
5	**0,977**

These values are very close to one for all transferences revealing that multilayers of this compound can be transferred, as has already said above.

As mentioned in the objectives of this work, the purpose of these studies is to fabricate the top contact electrode. In this sense, the experimental results detailed in the next paragraphs will demonstrate that annealing the films leads to the rupture of C-Au-

C bonds as has been already observed previously for solutions of MOC compounds by Chico et al.[33]. This process implies the reduction of gold(III) to gold(0) with the subsequent deposition of these gold nanoparticles (NPs) on top of the organic film while the -methoxy-isocyanidebencene group is eliminated by thoroughly rinsing the film with chloroform, scheme 3.1.

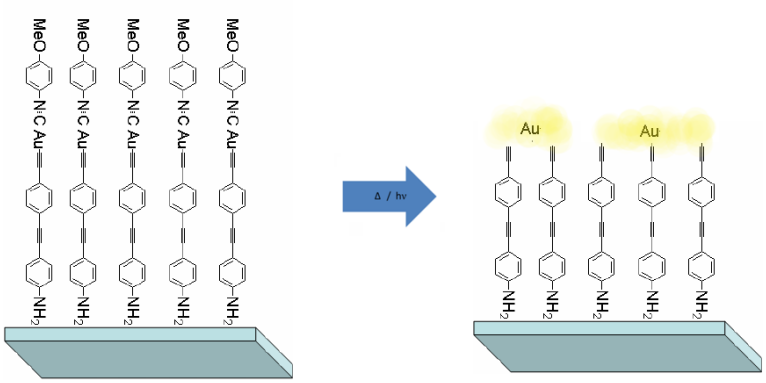

Scheme 3.1. Rupture of C-Au-C bonds after annealing and formation of gold NPs on the film surface. The 4-methoxy-isocyanidebencene group is eliminated by thoroughly rinsing the film with chloroform. The tolan group remains attached to the gold substrate by chemisorption of the amine group onto gold substrates.

A systematic study in which the films were annealed at different temperatures and during different periods of time was performed in Platon´s Group [34]. This study shown that the optimum conditions to fabricate the top contact electrode by annealing a organometallic compound by the rupture of the C-Au-C bond were to anneal the monolayer at 150 ºC during 2 hours. Therefore, these conditions were the used in this work to try to fabricate the top contact electrode with our compound.

QCM measurements were performed before and after the annealing process to verify the possible rupture of the C-Au-C bond. The variation of the frequency was Δf =13 Hz which would correspond to the loss of the 4-methoxy-isocyanidebencene group as is required to achieve our objective. Nevertheless, to be sure that this group is eliminated during the annealing process and that the reduction of gold(III) to gold(0) occurs experiments using XPS were performed.For XPS experiments, Langmuir films were transferred at a pressure of 14 $mN \cdot m^{-1}$ onto quartz substrates and keeping in a desiccators for 24 hours. In these experiments, our attention was focused on the nitrogen and gold atoms. Figure 3.5 shows the XPS spectra of MeOPhAu-Tolan-NH_2.

Figures 3.5a and b show XPS in N1s range before and after annealing. It can be appreciated that while Figure 3.5a shows two peaks at 400.04 and 399.12 eV corresponding to C≡N group and amine (NH_2) group, respectively; in Figure 3.5b only a peak at 399.89 eV is observed revealing the loss of the 4-methoxy-isocyanidebencene group.

On the other hand, in Figure 3.5c, Au4f region, two peaks at 84.09 and 87.77 eV are observed which correspond to gold(III). However, in Figure 3.5d, after annealing the film, we observe how the contribution of these peaks decreases and how two new peaks at at 87.16 and 83.54 eV appear. These new peaks are associated to the presence of gold(0) in the sample, so this result reveals the reduction of gold(III) to gold(0), although the reduction is not completed, and confirm the generation of gold nanoparticles onto the monolayer.

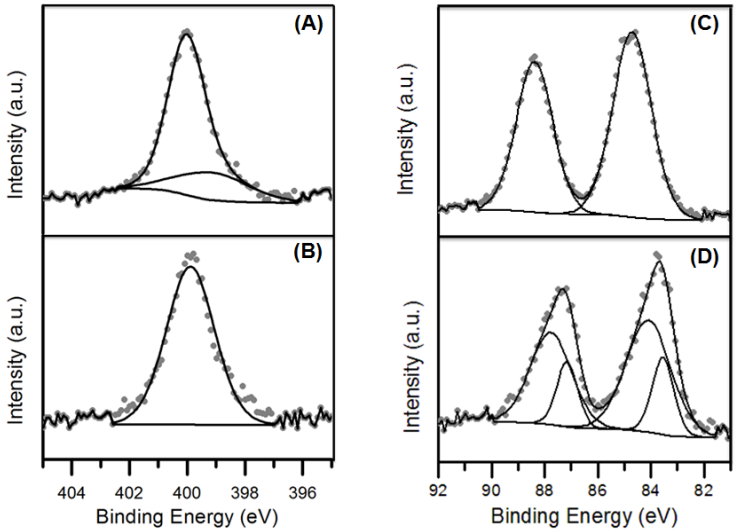

Figure 3.5 XPS spectra of MeOPhAu-Tolan-NH_2. (A) XPS in N1s range before annealing, (B) after annealing, (C) XPS in Au4f range before annealing and (D) after annealing.

Further evidence of the formation of gold NPs was provided by AFM and SEM experiments.

Figure 3.6 illustrates AFM images before and after the annealing process. As can be appreciated, there is a great presence of brightness spots and an increase of the roughness (RMS) once the annealing process had taken place which, together with the XPS results, reveal that gold NPs have been formed onto the molecular surface.

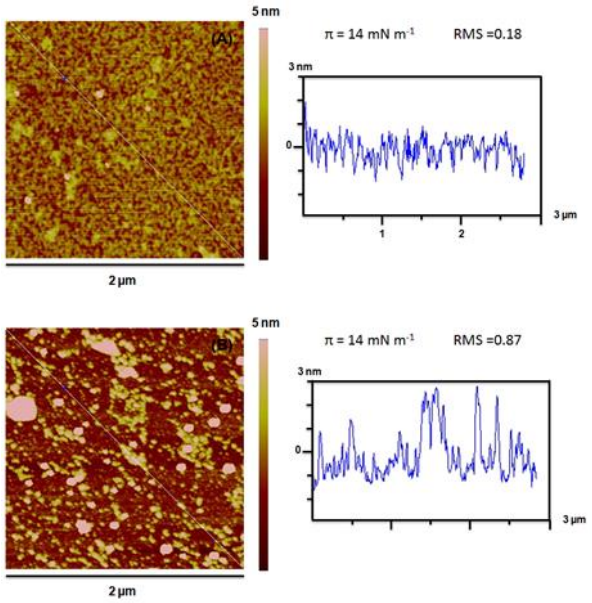

Figure 3.6 AFM images of MeOPhAu-Tolan-NH_2. Before (A) and after (B) annealing.

Finally, the images obtained with a SEM before and after the annealing process, Figure 3.7, also showed the presence of gold NPs in the monolayer, brightness spots are observed after annealing the sample in contrast with the absence of these for the image without annealing, Figure 3.7a.

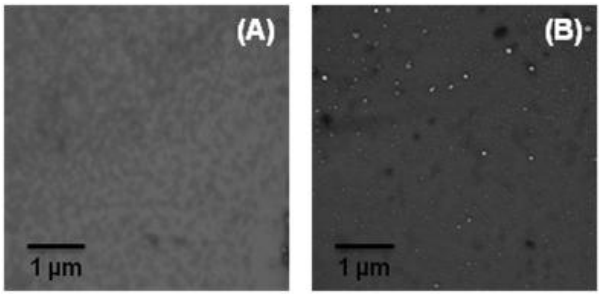

Figure 3.7 SEM images of MeOPhAu-Tolan-NH_2. Before (A) and after (B) annealing.

4 Deposition of a Metal layer by Stencil Lithography

This section reports the deposition of the top contact onto a monolayer without damaging the film by stencil lithography. The molecule chosen to form the monolayer, the stencil fabrication procedures, the evaporation procedure and some electrical measurements of the metal/molecule/metal devices are showed.

Shadow masks were firstly used in the prehistoric period where humans placed their hands over cave walls and blew a pulverized pigment around them. Nowadays, modern stencils have evolved many modes and have achieved sub-micrometer dimensions for nanotechnological applications. In addition, due to an increased in the demand of devices in the micro- and nano-meter scale patterning stencil lithography (SL) holds like a startling technique. This unique approach enables large scale micro and nano structuring of unconventional materials and on a large range of substrates which is not possible using conventional photolithography. Unconventional surfaces such as polymers, functionalized surfaces (e.g. self-assembled monolayers), 3D topographies, and mechanically unstable surfaces such as cantilevers and membranes can be patterned using this technique [35].

The resolution of the patters transferred depends on the setup configuration parameters. The stencil to source gap, material type, aperture size, deposition rate, and substrate temperature are some of the most influence characteristics to get a good patter [36]. The compound used was MeOPhAu-Tolan-NH_2 dissolved in chloroform to prepare a dissolution $5 \cdot 10^{-5}$ M. The preparation of the LB film carried out using the same procedure to it showed previously in chapter 3, but spreading a volume of 12.5 mL (1.25 $nm^2 \cdot molecules^{-1}$) and at surface pressure of transference of 14 $mN \cdot m^{-1}$and the layer was transferred onto gold substrates by the vertical dipping method.

Normally Finite Element Method is used to simulate membrane deformation caused by the deposited material. These models predict membrane deformation and aid in the determination of optimal stabilization schemes during the design phase of the process. Figure 4.1 illustrates the shadows of 3, 5, 10, 30 and 50 µm in diameter used in order to get information about the conductance of the metal-monolayer-metal system measured with a C-AFM as a function of the diameter of the top contact. Two different

designs were prepared: *Design a* in which all the sized apertures are in one aperture membrane and *design b* in which each membrane has only a diameter size.

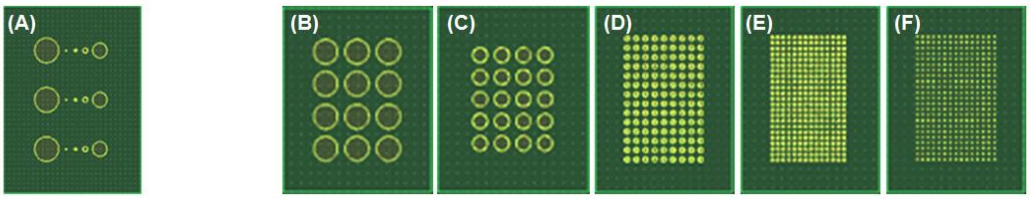

Figure 4.1. Designs of the stencils. (A) design a; (B), (C), (D), (E) and (F) design b.

These stencils shadows were prepared by CNM´s technicians as following:

Firstly, a layer of silicon nitride (SiN), 120-300 nm, was deposited by low-pressure chemical vapor deposition (LPCVD) onto both sides of a silicon wafer. After that, a 1µm layer of aluminum was sputtered onto the back side to protect the SiN layer of this side.

Once completed that process, a photoresist was deposited on the front side (face in contact with the molecular layer during the evaporation process) and the apertures were formed by photolithography. Then, reactive ion etching (RIE) produces the apertures of the stencil on the SiN layer and finally, the photoresist was striped.

The next step was to deposit a photoresist in the back side to define the membrane by photolithography. After that, the Al layer of this side was eliminated by

inductively coupled plasma (ICP). At this point, a deep reactive ion etching (DRIE) of SiN and Si was done leaving a layer of silicon of approximately 100 µm.

At this moment, it is necessary to cut the wafer onto little chips to avoid breaking the stencils.

Finally, the membranes were released by a KOH attack. First of all, the chip was dipped in a hydrofluoric acid solution (5% weight) during 15 seconds to remove the oxide layer in a Teflon® recipient. This attack was stopped by a water cascade during 5 minutes. Afterward, a bathroom in KOH (40% weight) at 75 °C (conditions optimized for smooth surfaces) was prepared in a Teflon® container with a considerable volume to allow regeneration of ions. An etch rate of about 1.56 $\mu m \cdot h^{-1}$ is obtained. After 3 hours, the chips were cleaned with water and ethanol for 5 minutes.

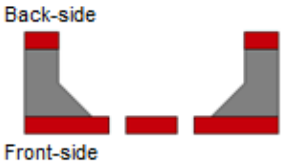

In Figure 4.2 we can see the stencils obtained following the fabrication process mentioned above. Nevertheless, in a future work, smaller stencils can be prepared following the scheme showed in Appendix 1. . It is necessary to note here that a new fabrication process is being optimized to get that the smallest shadows open before the biggest ones break due to the stress. Figure 4.2a (design a) shows several size shadows (50, 30 and 10 µm). Nevertheless, during the evaporation process only through 50 µm patters the metal was transferred onto the molecular layer. Meanwhile in the design b (Figure 3-2b,c and d) all shadows (10, 30 and 50 µm) allow to the metal pass during the evaporation process.

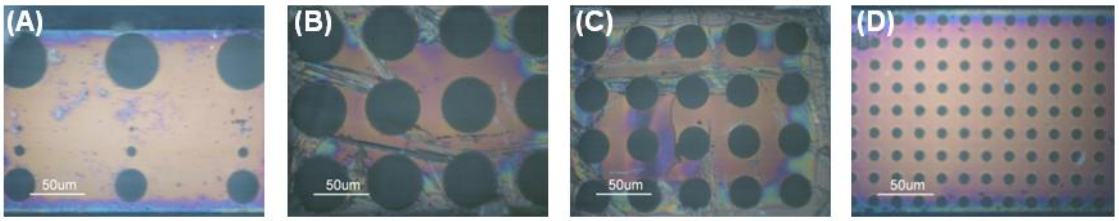

Figure 4.2. Stencil apertures; (A) design a; (B), (C) and (D) design b.

Once the substrates and stencils were fabricated, the evaporation process was carried out. Figure 4.3 shows how the shadow was located onto the substrates with the molecular layer before and after the evaporation process.

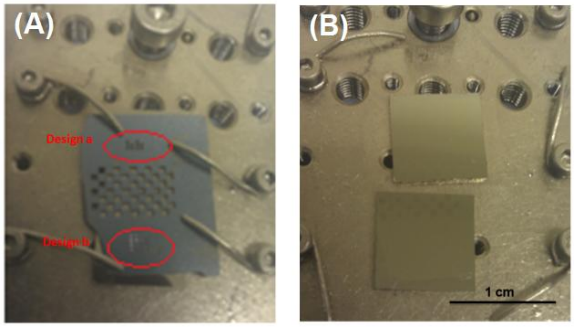

Figure 4.3. Images before and after the evaporation process onto the gold substrates with the monolayer.

The evaporation pressure was $2.43 \cdot 10^{-5}$ mbar. The gold was evaporated and deposited at a rate of 0.15 $nm \cdot s^{-1}$ to get a layer of 20 nm. In Figure 4.4 we can see, by optical microscopy, the top contacts transferred by the shadows of stencil design b onto the LB film.

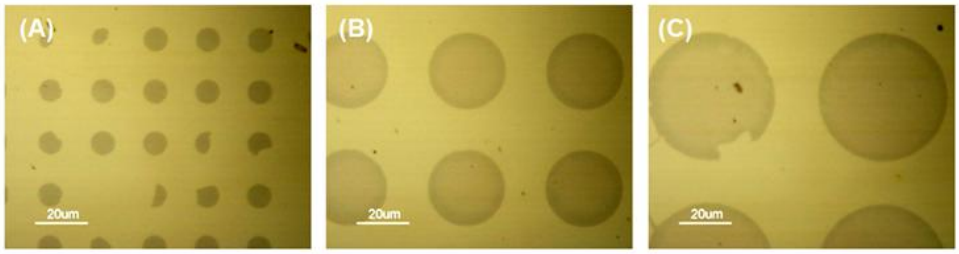

Figure 4.4. Top contact images. (A) 10 µm, (B) 30 µm, and (C) 50 µm in diameter.

Once the metal/molecule/metal devices were prepared the next stage was to perform electrical measurements on those using a C-AFM in contact mode. To ensure the reproducibility of the results I-V curves were obtained at different localizations on the sample and several samples were used. The tip was a SCM platinum-iridium, the scan rate was 0.50 Hz and the set point 1.2 V. The curves were performed from -4 to +4V.

Figure 4.5 shows the I-V curves performed onto a gold substrate without molecules, onto a molecular surface and onto a gold top contact electrode. When the tip is onto a bare gold substrate (without molecules) the current increases rapidly as the voltage moves away from zero value (blue line); this I-V curve is typical of conductor materials. If the tip is located onto a molecular film, a flat profile is obtained for the I-V curve meaning that the molecular film behaves as an insulate (green line). Finally, when the tip is onto a top electrode formed by stencil lithography an intermediate situation is obtained (red line).

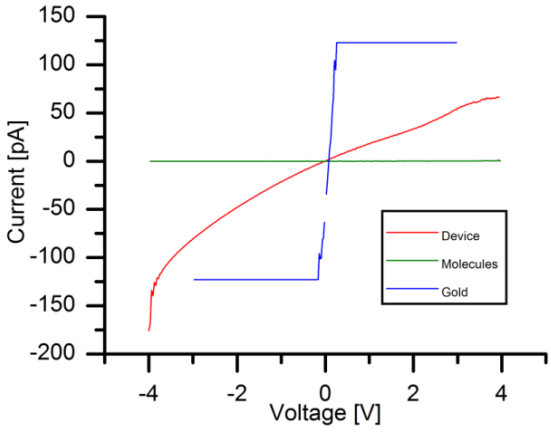

Figure 4.5. I-V curves obtained for a bare substrate (blue line), onto a molecular film (green line) and onto a gold top contact fabricated by stencil lithography (red line).

The same I-V curves (red line in Figure 4.5) were obtained independently of the top contact size (shadow size) and also even when the tip was located between two fabricated top contacts (Figure 4.4). Moreover the same sigmoidal profile obtained in other experiments in the Platon group [37] is not obtained. Additionally the intensities obtained are two orders of magnitude lower than expected.

5 Graphene Oxide

In this section, fabrication of graphene oxide (GO) layers by the LB method is showed and consequently its possible uses in the fabrication of the top-contact electrode by transference onto a substrate and subsequent reduction. This work is focused in graphene oxide because allow to obtain graphene by reduction and because this material can be assembled by the Langmuir-Blodgett technique. Thus, in this section the surface pressure-area isotherms, BAM and AFM images are presented and discussed.

Graphene is a two dimensional promising material composed by a monolayer of sp^2 bonded carbon atoms which has attracted a great interest since in 2004 was discovered by A. K Geim and K.S Novoselov [38]. The extraordinary properties of the graphene are well-known, so graphene has a huge intrinsic mobility (up to $2 \cdot 10^{-5}$ cm^2 $V^{-1}s^{-1}$ at room temperature), which implying a low intrinsic resistivity at room temperature, 10^{-6} $\Omega \cdot cm$ [39-40]; its high specific surface area (~2600 m^2g^{-1}) [41] becomes graphene in a potential candidate for developing high sensitive sensors (gases [42], biosensors, [43], …); and its high conductivity and specific surface area becomes it as a possible successor of graphite in the fabrication of anodes ion-lithium batteries [44]. Also, graphene has the highest thermal conductivity (~5000$Wm^{-1}K^{-1}$) [45] and its exceptional mechanical properties become graphene in the most resistant material (traction tough of 130 GPa, and Young modulus ~1.0 TPa) [46]. In addition, the optical properties of graphene revealing a hopefully future in a large number of applications as a transparent conductive electrode due to its optical transmittance (~ 97.7%) independent of wave length; and its high electrical conductivity.

Nevertheless, the manipulation of graphene is not easy so other similar materials are required to take advantage of the incredible properties of graphene. In this work, graphene oxide (GO) was used as an alternative to the graphene since this material can be assembled by LB technique (GO layers, which are hydrophilic, can form stable and homogeneous colloidal suspensions in aqueous and/or polar organic solvents due to the negative electrostatic repulsions between layers) and convert to graphene by reduction, as it has been said above. In addition, GO is considerate as a promising material for polymer composite and transparent conductors due to their scalability production. GO is composed by a carbon hexagonal network of covalently linked carbon atoms with

functional groups containing oxygen attached to various sites; carboxylic acids at the edges, and hydroxyl or epoxide groups at the basal plane, Figure 5.1. These dispersions can be processed and assembled by spin and spray coating [47], transfer printing [48], dip-coating [49], electrophoretic deposition [49] or Langmuir-Blodget technique [50]; method used in this work

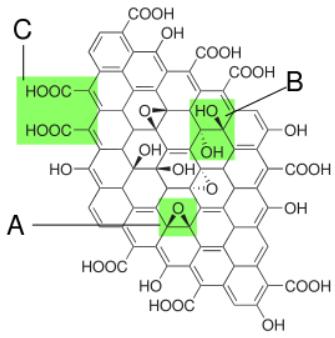

Figure 5.1 Schematic representation of the structure of a GO layer. Hydroxyl groups and epoxy disrupt electron conjugation graphitic network through sp3 bond formation.

Dispersions of GO 8.8 mg/L in 5:1:6; methanol:water:chloroform or ethanol:water:chloroform (which were sonicated during 5 minutes before spreading) were used to assemble this material by LB technique, Figure 5.2 shows a representative surface pressure-area (π-*A*) isotherm of both GO dispersions at the air-water interface.

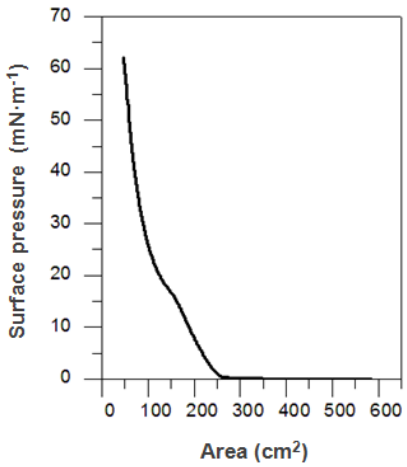

Figure 5.2. Surface pressure $mN{\cdot}m^{-1}$ vs. area (π-A) isotherm of both GO dispersions at the air-water interface.

As can be observed, four stages well differentiated and defined by changes in the slope are obtained. First stage, from 600 to 250 cm^2 correspond to a gaseous phase

where there are not interactions between the GO sheets. During the second one, from 250 to 190 cm^2, the surface pressure starts to increase upon compression revealing first interactions between GO sheets. From 190 to 120 cm^2 other slope change is observed, third stage, in which BAM image (Figure 5.3) shows a packed stage although with areas without covering and how some sheets start to fold at the touching points along their edges (instead of overlapping) [50]. Finally, from 120 to 46 cm^2 BAM image shows how the monolayer cover practically all the interface although GO sheets continue overlapping and wrinkling.

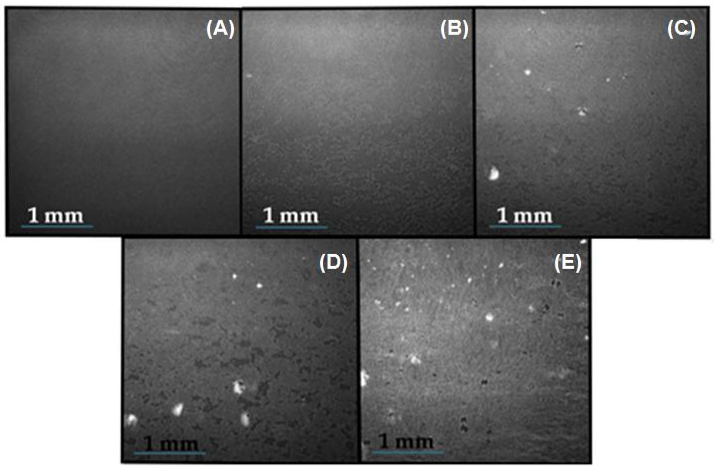

Figure 5.3 BAM images of GO dispersions at the air-water interface (A) and (B) correspond to the first stage, (C) to the second stage, (D) to the third one and (E) to the fourth stage.

Once observed and studied the formation of a Langmuir film of GO at the air-water interface, the next step was to transfer the monolayer onto a substrate (mica) and to check the morphology of the film by AFM. Taking into account the isotherm, three different surface pressures were selected to make the transference: 5, 20 and 35 $mN \cdot m^{-1}$.

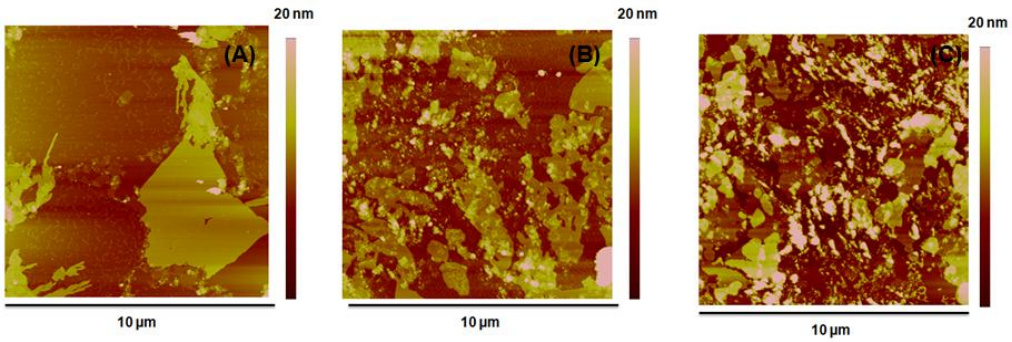

Figure 5.4. AFM images of a LB film of GO transferred at (A)5 $m \cdot Nm^{-1}$ (B) 20 $m \cdot Nm^{-1}$ and (C) 35 $m \cdot Nm^{-1}$.

Figure 5.4 shows the recorded AFM images. At 5 $mN \cdot m^{-1}$, Figure 5.4a, we can observe the presence of single GO sheets as well as large sheets, around 12 μm^2, which are not monolayers. As surface pressure increases, 20 $mN \cdot m^{-1}$, GO sheets start to close existing interactions between them, Figure 5.4b, and the sheets are folded since these are soft and flexibl5 $mN \cdot m^{-1}$e and start to wrinkly and overlap. Finally, at a surface pressure of 35 $mN \cdot m^{-1}$, Figure 5.4c, a great number of winkling sheets, folding points and some sheets overlapping were observed.

Due to not formation of a monomolecular film as it has been observed in Figure 5.4, a new spreading process using a GO dispersion in solvents with more purity was carried: ethanol:water:chloroform (5:1:6) or methanol:water:chloroform (5:1:6) and the Lamguir film was transferred at 15 $mN \cdot m^{-1}$ onto a mica to be studied by AFM, Figure 5.5 and Figure 5.6, respectively. The image in Figure 5.5 shows large GO sheets composed by several layers (a monolayer has a tickness of 1 nm), see section analysis in Figure 5.5, and also the presence of impurities due to probably a pieces of small GO sheets or rest of the solvents which were yet observed in Figure 5.4. The same result was obtained when GO was solved in a more pure methanol:water:chloroform (5:1:6) mixture, see Figure 5.6.

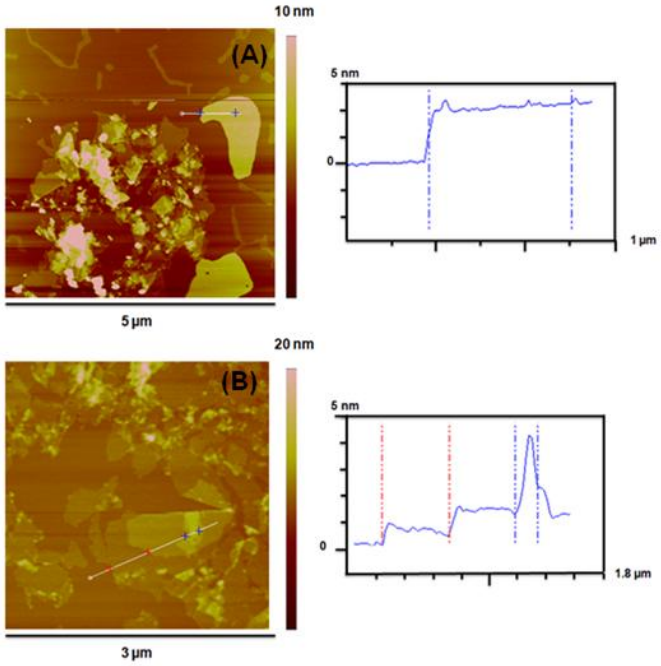

Figure 5.5. AFM image of a LB film of GO transferred at 15 $mN \cdot m^{-1}$ using more pure solvents: (A) ethanol:water:chloroform (5:1:6); (B) methanol:water:chloroform (5:1:6).

6 Conclusions

We can conclude that the three different methods studied in this work for the fabrication of the top contact electrode in metal/molecule/metal devices reveal that the three routes are feasible and promising to achieve the objective. Although the three ones are in a different level of development and need a further work.

Nevertheless, the main conclusions obtained from this work are:

The ***Rupture of a MOC*** has permitted to fabricate a metal/molecule/metal device being an efficient method for the fabrication of the top contact electrode and minimizing the appearance of short circuits which are a rather common problem in other traditional methods used for the metallization of monolayers.

In addition, this technique avoids expensive and damage deposition techniques for the fabrication of the top contact electrode such as chemical vapour deposition (CVD) or atomic layer deposition (ALD). Although electrical measurements need to be performed to test the real effectiveness of the method.

The use of ***Stencil technique lithography*** as possible method to fabricate the top contact electrode has concluded that:

i) I-V curves not depend on the size of the top electrode in contrast to the expected.

ii) The gold substrate roughness does not allow good electrical measurements. Nevertheless, this roughness does not explain the different I-V curves obtained depending on the placement of the tip and why the same I-V curve is performed for all the top-electrode sizes.

iii) Damage of the layer during the evaporation process. Although the evaporation process is fast the temperature reached in the chamber can damage the layer.

iv) Generation of little short-circuits. Even when the probabilities of generating a short-circuit decreases by SL, the energy of the gold atoms evaporated which pass through shadows and reach the molecular layer could be high enough to create bridges between the top and bottom electrode (red line).

Finally, the use of ***GO as possible top contact electrode*** has concluded that GO can be transferred onto solid substrates using LB technique; although an optimization of the conditions is required to get homogenous GO sheets which can be reduced to form graphene without damaging the film and, thus, can be used as a top-contact electrode.

Appendix 1

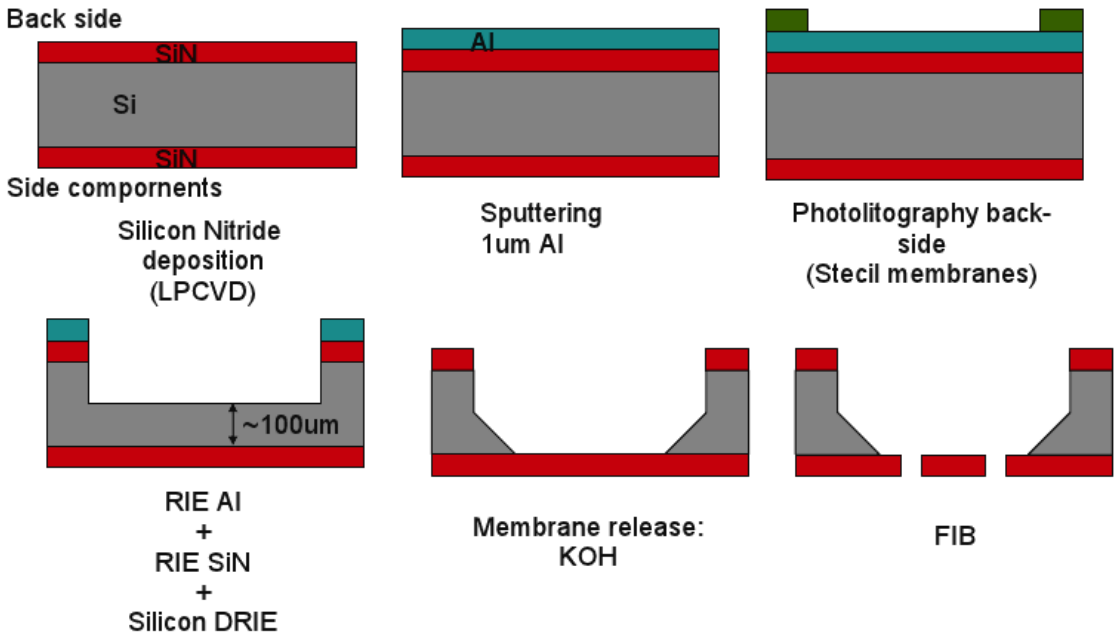

Acknowledgements

Jorge Trasobares Sánchez, NANOMAT master student in the academic year 2011-12, is grateful for financial assistance from INTERREG IV B SUDOE; Transpyrenees Action on Advanced Infrastructures for Nanosciences and Nanotechnologies TRAIN2; and Ministerio de Ciencia e Innovación (grant number: 5108900).

Special gratitude to Dr. Pilar Cea and Dr. Santiago Martin Solans, supervisors of this work. It has been a pleasure to work with you at this time. Also special thanks to PhD students Luz Mariana and Javier Cortes and to Platon´s Group for your support and companionship.

Thanks to Dr. Wolfgang Maser, Dr. Ana Benito and Dr. Pere Castell from Instituto de Carboquímica of Zaragoza by providing "GO" samples and by the helpful meetings.

Thanks to Dr. Francesc Pérez Murano and his group Lorea Oria, Marc Sansa and Nerea Alayo for your welcome to the CNM and useful meetings. It was a pleasure to meet you and share your knowledge.

References

[1] André-Yves Portnoff, "Claves para el Nanomundo", *Cotec*, 27,**2008**.

[2] M. L. Grieneisen, M. Zhang, *Nature Nanotechnology* , 7, 273, **2012**.

[3] http://en.wikipedia.org/wiki/History_of_nanotechnology

[4] G. A. Waychunas, *Reviews in Mineralogy and Geochemistry*, 44, **2001**.

[5] Foundation Phantoms, "Un análisis de la situación presente y de las perspectivas de futuro", **2008**.

[6] N. J. Tao, *Nature Nanotechnology*, 1, 173, **2006**.

[7] G. E. Moore, *Electronics*, 38, **1965**.

[8] http://www.itrs.net

[9] A. M. Ionescu, "Nanoelectronics roadmap: evading Moore's law".

[10] Y.Taur, D. A. Buchanan, W.Chen, D. J.Frank, K. E. Ismail, S. H. Lo, G. A.Sai-Halasz, R. G.Viswanathan, H. J. C. Wann, S. J Wind, *Proceedings of the IEEE*, 85, 486, **1997**.

[11] T. F.Heinz, H. W. K. Tom, Y. R. Shen, *Physical Review A*, 28, 1883, **1983**.

[12] A. G. A. MacDiarmid, *Angewandte Chemie International Edition*, 40, 2581, **2001**.

[13] H. A. Shirakawa, *Angewandte Chemie International Edition*, 40, 2575, **2001**.

[14] J. C. S. Cuevas, E. En *World Scientific: Singapore; Hackensack, NJ*, 1, 3, **2010**.

[15] J. R. Heath, M. A. Ratner, *Physics Today*, 56, 43, **2003**.

[16] C. Silien, M. Buck, *Journal of Physical Chemistry C*, 112, 3881, **2008**.

[17] T.Xu, I. R. Peterson, M. V. Lakshmikantham, R. M. Metzger, Angewandte, *Journal of Physical Chemistry B*, 105, 7280, **2001**.

[18] T. Xu, I. R. Peterson; M. V. Lakshmikantham,.; R. M. Metzger, *Angewandte Chemie International Edition*, 40, 1749, **2001**. Tao Xu,

[19] D. A.Antelmi, J. N. Connor, R. G. Horn, *Journal of Physical Chemistry B*, 108, 1030, **2004**.

[20] F. Von Wrochem, D. Gao, F. Scholz, H. G. Nothofer, G. Nelles, J. M. Wessels, *Nature Nanotechnology*, 5, 618, **2010**.

[21] H. B. Akkerman, P. W. M. Blom, D. M. De Leeuw, B. De Boer, *Nature Nanotechnology*, 441, 69, **2006**.

[22] T. Li, J. R Hauptman, Z. M. Wei, S. Petersen, N. Bovet, T.Vosch, J. Nygard, W. P. Hu, Y. Q. Liu, T. Bjornholm, K. Norgaard, B.W. Laursen, *Advanced Materials*, 24, 1333, **2012**.

[23] G.Wang, Y. Kim, M. Choe, T. W. Kim, T. Lee, *Advanced Materials*, 23, 755, **2011**.

[24] A. Vilan, D. S. Cahen, , *Advanced Functional Materials*, 12, 795, **2002**.

[25] K. T. Shimizu, J. D. Fabbri, J. J. Jelincic, N. A. Melosh, *Advanced Materials*, 18, 1499, **2006**.

[26] N.Stein, R. Korobko, O. Yaffe, R. Har Lavan, H. Shpaisman, E. Tirosh, A. Vilan, Cahen, D. Nondestructive, *The Journal of Physical Chemistry C*, 114, 12769, **2010**.

[27] A. P. Bonifas, R. L. McCreery, *Nature Nanotechnology*, 5, 612, **2010**.

[28] T. Kuilla, S. Bhadra, D. Yao, N. H. Kim, S. Bose, J. H. Leea, *Progress in Polymer Science*, 35, 1350, **2010**.

[29] L. Wilhelmy, *Annals of Physics*, 177, 119, **1863**.

[30] D. M. Hönig, D., *Journal of Physical Chemistry B*, 95, 4590, **1991**.

[31] http://en.wikipedia.org/wiki/Snell's_law

[32] Sauerbrey, G. Zeitschrift fur Physik, 206, 155, **1959**.

[33] R. Chico, E. Castillejos, P. Serp, S. Coco, P. Espinet, *Inorganic Chemistry*, 50, 8654, **2011**.

[34] J. C. Cameros, "Preparación de películas de Langmuir y de Langmuir-Blodgett. Determinación de su estructura y aplicaciones", *TAD. Universidad de Zaragoza*, **2012**.

[35] M. A. F. v. d. Boogaart, "Stencil lithography: An ancient technique for advanced micro- and nanopatterning", *Ecole Polytechnique Fédérale de Lausanne (EPFL); Institute of Microelectronics and Microsystems (IMM); Laboratory of Microsystems and Nanoengineering (LMIS1),* **2006**.

[36] http://spie.org/x45083.xml

[37] L. M. Ballesteros, C. Momblona, S. Marqués-González, M. C. López, R. J. Nichols, P.J. Low, and P. Cea, *The Journal of Physical Chemistry C,* 116, 9142, **2012**.

[38] P. S. Fernández, "Modificación superficial de materiales de carbono: grafito y grafeno", *Departamento de Ciencia de los Materiales e Ingeniería Metalúrgica. Universidad de Oviedo,* **2011**.

[39] S.V. Morozo, K.S. Novoselov, M.I. Katsnelson, F. Schedin, D.C. Elias, J.A. Jaszczak, A.K. Geim, *Physical Review Letters*, 100, 016602, **2008**.

[40] J.H. Chen, C. Jang, S. Xiao, M. Ishigami, M.S. Fuhrer, *Nature Nanotechnology*, 3, 206, **2008**.

[41] S. Stankovich, D.A. Dikin, G.H.B. Dommett, K.M. Kohlhaas, E.J. Zimney, E.A. Stach, R.D. Piner, S.T. Nguyen, R.S. Ruoff, *Nature Nanotechnology*, 442, 282, **2006**.

[42] F.Schedin, A.K. Geim, S.V. Morozov, E.W. Hill, P. Blake, M.I. Katsnelson, K.S. Novoselov, *Nature Materials*, 6, 652, **2007**.

[43] C. Shan, H. Yang, J. Song, D. Han, A. Ivaska, L. Niu, *Anaitical Chemistry* , 81, 2378, **2009**.

[44] E. Yoo, J. Kim, E. Hosono, H.s. Zhou, T. Kudo, I. Honma, *Nano Letters*, 8, 2277, **2008**.

[45] A.A. Balandin, S. Ghosh, W. Bao, I. Calizo, D. Teweldebrhan, F. Miao, C.N. Lau, *Nano Letters*, 8, 902, **2008**.

[46] C.Lee, X. Wei, J.W. Kysar, J.Hone, *Science*, 321, 385, **2008**.

[47] Y. Zhu, S. Murali, W. Cai, X. Li, J. W. Suk, J. R. Potts, R. S. Ruoff, *Advanced Materials*, 22, 3924, **2010**.

[48] S. J. Wang, Y. Geng, Q. B. Zheng, J. K. Kim, *Carbon*, 48, 1815, **2010**.

[49] X.Wang, L. J. Zhi, K. Mullen, *Nano Letters*, 8, 323-327, **2008**.

[50] Q. Zheng, W. H. Ip, X. Lin, N. Yousefi, K. K. Yeung, Z. Li, J.K. Kim, *ACS Nano*,. 5, 6039, **2011**.